Journal of Power Sources 240 (2013) 772–778

Contents lists available at SciVerse ScienceDirect

Journal of Power Sources

journal homepage: www.elsevier.com/locate/jpowsour

In-situ neutron diffraction study of the $xLi_2MnO_3\cdot(1-x)LiMO_2$ ($x = 0, 0.5$; M = Ni, Mn, Co) layered oxide compounds during electrochemical cycling

Haodong Liu [a], Christopher R. Fell [b], Ke An [c], Lu Cai [c], Ying Shirley Meng [a,*]

[a] Department of NanoEngineering, University of California San Diego, La Jolla, CA 92121-2460, USA
[b] Global Technology & Innovation, Power Solutions, Johnson Controls, Inc., Milwaukee, WI 53209, USA
[c] Chemical and Engineering Materials Division, Oak Ridge National Laboratory, Oak Ridge, TN 37830, USA

HIGHLIGHTS

- Pouch cells have been built for *in-situ* neutron diffraction study.
- *In-situ* neutron diffraction was performed on layered oxide compounds.
- *Ex-situ* neutron powder diffraction was performed on Li-excess layered compounds.
- The dynamic changes in both cathode and anode have been observed simultaneously.

ARTICLE INFO

Article history:
Received 25 February 2013
Received in revised form
27 April 2013
Accepted 29 April 2013
Available online 13 May 2013

Keywords:
Lithium-ion battery
In-situ neutron diffraction
Layered oxide cathode
Graphite anode

ABSTRACT

The layered oxide compounds $xLi_2MnO_3\cdot(1-x)LiMO_2$ (M = Ni, Mn, Co) are of great interest as positive electrode materials for high energy density lithium-ion batteries. *In-situ* neutron diffraction was carried out to compare the structural changes between the classical layered compound $Li[Ni_{1/3}Mn_{1/3}Co_{1/3}]O_2$ ($x = 0$) and lithium-excess layered compound $Li[Li_{0.2}Ni_{0.18}Mn_{0.53}Co_{0.1}]O_2$ ($x = 0.5$) during electrochemical cycling. In this work, lab made pouch cells were built for the *in-situ* study and graphite was used as the anode material. Irreversible structural change of $Li[Li_{0.2}Ni_{0.18}Mn_{0.53}Co_{0.1}]O_2$ during first charge (4.7 V)/discharge cycle (2.0 V) was indicated by dynamic changes in lattice d-spacing, while the $Li[Ni_{1/3}Mn_{1/3}Co_{1/3}]O_2$ showed completely reversible structural evolution between 4.4 V and 2.5 V. *Ex-situ* neutron powder diffraction was performed on both pristine and chemically delithiated lithium-excess layered compounds to better understand the irreversible structure change.

1. Introduction

Rechargeable lithium-ion batteries play a significant role in many portable devices such as laptops and cell phones. They are emerging as the energy storage systems for electric vehicles because of high energy density and long cycle life. The layered oxide compounds $xLi_2MnO_3\cdot(1-x)LiMO_2$ (M = Ni, Mn, Co) are of great interest as a new generation of positive electrode materials for high energy density lithium-ion batteries because of their high energy density at lower costs. The currently commercialized $LiNi_{1/3}Mn_{1/3}Co_{1/3}O_2$ ($x = 0$) cathode material, has firstly been reported to have a capacity of 150 mAh g^{-1} in the voltage window of 2.5–4.2 V by Ohzuku et al., [1] and 200 mAh g^{-1} in the voltage window of 2.5–4.6 V. [2] S.C. Yin et al. suggests an upper cutoff voltage of 4.3–4.4 V for good cycling retention, as their observation shows that in this voltage window Lithium de/re-intercalation is reversible. [3] Recently, there is an intense research effort focused on the Lithium excess material $xLi_2MnO_3\cdot(1-x)LiMO_2$ (in $LiMO_2$, M = Ni, Mn, Co) where $x > 0$, which has excess Li in the transition metal layer. The X-ray diffraction pattern of the layered oxides can be refined with the α-$NaFeO_2$ structure (R-3m) [1–3]. Superlattice peaks exist in the X-ray diffraction pattern between 20 and 25° (2θ), which are associated with a honeycomb ordering of Li^+, Ni^{2+}, Mn^{4+}, and Co^{3+} in the transition metal layer [4,5]. The Lithium-excess materials can deliver reversible capacities in excess of 250 mAh g^{-1} when the x is close to 0.5 [6–8], but large irreversible capacity up to ~100 mAh g^{-1} exists in the first charge and discharge between 2 V and 4.8 V, several groups have proposed detailed mechanisms for this large irreversible capacity [9,10].

* Corresponding author.
E-mail address: shirleymeng@ucsd.edu (Y.S. Meng).

0378-7753/$ – see front matter © 2013 Published by Elsevier B.V.
http://dx.doi.org/10.1016/j.jpowsour.2013.04.149

During the initial charging region in first cycle, as lithium is removed from the layered structure the capacity originates from the oxidation of Ni^{2+} to Ni^{4+} and Co^{3+} to $Co^{3.6+}$ up to 4.4 V. A high voltage plateau region around 4.5 V appears after the slope region. The large first cycle irreversible capacity has been mainly attributed to an irreversible loss of oxygen from the lattice during the first charge accompanied by Li removal. It is also a result of side reactions with the electrolyte on the electrode surface [7,9,11]. However, it is still up to debate where the anomalous high reversible capacity comes from in the lithium excess layered oxides. In order to gain more in-depth insights about the differences in classical layered oxide ($x = 0$) and lithium excess layered oxide ($x = 0.5$), *in-situ* neutron diffraction experiments were designed to observe the structural and compositional changes in these oxides during electrochemical process.

Previous literature has focused heavily on the use of X-ray scattering to understand the structural evolution of these materials. Recently, an *in-situ* XRD study has been done on the Li$[Li_{0.2}Ni_{0.2}Mn_{0.6}]O_2$ to investigate the structural change and mirco-strain during the first electrochemical cycle [12]. In addition, an *in-situ* XAS experiment was performed on the Li$[Ni_{0.17}Li_{0.2}Co_{0.07}Mn_{0.56}]O_2$ to study the charge–discharge reaction mechanism in the first 2 cycles [13]. However, X-ray scattering is limited in that it interacts with the electrons surrounding the atoms making it difficult for Li-ion battery compounds, whereas neutron interacts with the atomic nuclei of materials. Neutron scattering has several distinct advantages over X-ray scattering for *in-situ* battery studies [14]: 1) Deep penetration that allows simultaneous observation of the cathode and anode; 2) Larger scattering contrast between neighboring elements in the periodic table specifically the scattering lengths, e.g. for transition metals in this case: Ni, 10.3 fm; Mn, −3.73 fm; Co, 2.49 fm; [3] and 3) The sensitivity to light elements such as Li is significant in order to estimate their position in the crystal structure. However, due to the large incoherent neutron-scattering cross-section of hydrogen, the existence of hydrogen is detrimental to the signal-to-noise ratio of neutron diffraction pattern. Separators (polyethylene based porous membrane) and poly carbonate based electrolyte solutions contain large amount of hydrogen. This poses a significant challenge to *in-situ* neutron diffraction for lithium ion battery research although it is such a powerful technique.

The number of *in-situ* ND studies are limited and have focused on traditional materials such as $LiCoO_2$ [14,15], $LiMn_2O_4$ [16,17], $Li_4Ti_5O_{12}$ [18] and graphite [19]. In order to avoid large absorption from the presence of hydrogen in the separator and electrolyte, most studies use a special designed electrochemical cell [14–16,18,19]. In this work, lab made pouch cell were designed for *in-situ* ND study. Both $LiNi_{1/3}Mn_{1/3}Co_{1/3}O_2$ and Li$[Li_{0.2}Ni_{0.18}Mn_{0.53}Co_{0.1}]O_2$ materials are studied by *in-situ* neutron diffraction during electrochemical cycling on the engineering materials diffractometer VULCAN (see the references), at Spallation Neutron Source, Oak Ridge National Laboratory. The structural transition behaviors of the two cathode compounds during the first few cycles are presented. Structure change and phase transition of anode graphite is also discussed briefly in this article.

2. Experimental methods

2.1. Synthesis

A coprecipitation followed by two steps calcination was used for the synthesis of the materials [20]. Transition metal (TM) nitrates, $Ni(NO_3)_2 \cdot 6H_2O$ (ARCROS, 99%), $Co(NO_3)_2 \cdot 6H_2O$ (ARCROS, 99%), and $Mn(NO_3)_2 \cdot 4H_2O$ (Alfa Aesar, 98%) were dissolved into deionized water then titrated into $LiOH \cdot H_2O$ (Fisher) solution. The coprecipitated TM hydroxides were then filtered using vacuum filtration and washed three times with deionized water. The collected TM hydroxides were dried in an oven at 180 °C for 10 h in air. The dried TM precursors were then mixed with a stoichiometric amount of $LiOH \cdot H_2O$ (Fisher) corresponding to the amount of $M(OH)_2$ from the coprecipitation step. This mixture was ground for 30 min to ensure adequate mixing and then placed into a furnace at 480 °C for 12 h. The precalcinated powders were then calcinated at 900 °C for 12 h in air.

Chemical delithiations were performed in a glovebox (argon atmosphere) with <1 ppm moisture, $Li_{1.2}Ni_{0.2}Mn_{0.6}O_2$ was mixed with the designed amount of NO_2BF_4 (ARCROS, 97%) in acetonitrile (Alfa Aesar, 99.8%) and stirred for 24 h, then filtered.

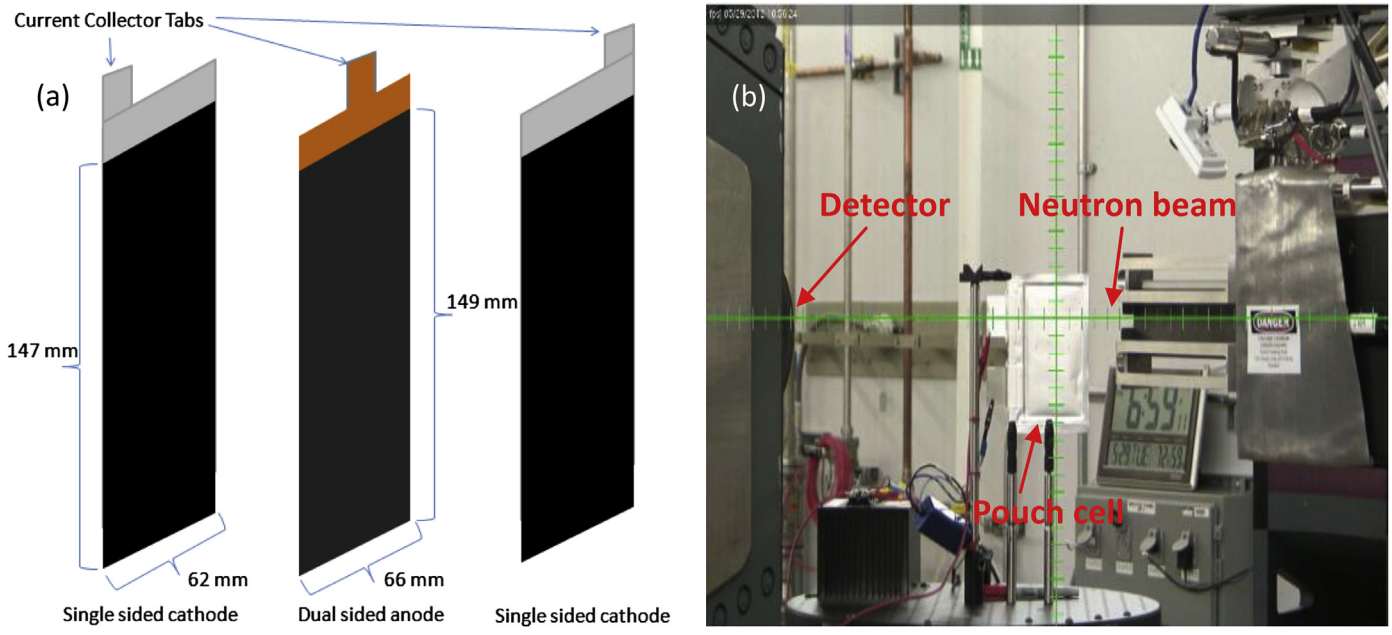

Fig. 1. (a): Simple schematic of lab made pouch cell for *in-situ* neutron diffraction study; (b): Pouch cell installed on VULCAN beamline.

2.2. Cell design

Fig. 1a is a simple schematic of our pouch cell, which includes a dual sided graphite anode (the anode is based on standard graphite material) and two pieces of single side cathode. The electrode loading for the anode and $Li[Li_{0.2}Ni_{0.18}Mn_{0.53}Co_{0.1}]O_2$ cathode is around 8 mg cm^{-2}, while the loading for $LiNi_{1/3}Mn_{1/3}Co_{1/3}O_2$ cathode is around 12 mg cm^{-2}. This cell configuration design aimed at increasing the loading of active materials in our pouch cells to increase neutron diffraction pattern statistics. Cells were all assembled in a glovebox under argon atmosphere. A Celgard separator is used to cover the anode with a piece of single side cathode on each side of the anode. The electrolyte solution composed of 1 M $LiPF_6$ in a 1:1 ethylene carbonate (EC):dimethyl carbonate (DMC). The cathode is composed of 90% active material, 5% PVDF and 5% carbon black on an aluminum collector. In order to ensure the full charge performance of the cathode materials, about 25% excess anode material was used in the pouch cell.

2.3. In-situ neutron diffraction

A Bio-Logic SP-300 potentiostat was used to electrochemically cycle the cell under constant charge and discharge currents. The $Li[Li_{0.2}Ni_{0.18}Mn_{0.53}Co_{0.1}]O_2$/C pouch cell was charged at 32 mA (~C/15) to 4.7 V then discharged at −27 mA (~C/15) to 2 V while the $LiNi_{1/3}Mn_{1/3}Co_{1/3}O_2$/C pouch cell was charged at 43.2 mA (~C/5) to 4.4 V then discharged at −43.2 mA (~C/5) to 2.5 V. In order to observe more cycles within the limited beam time, the following cycles between a voltage range of 2.5–4.4 V were using ±84 mA (~C/2) to charge and discharge. Fig. 1b is the cell setup at the VULCAN beamline. An incident beam (5 mm × 12 mm) of 0.5–3.5 Å bandwidth allowing 0.5–2.5 Å d-space in diffracted pattern in the $\theta \pm 90^\circ$ detector bank was selected using the double-disk choppers at 30 Hz speed. The SNS was at nominal 800 KW. Time stamped neutron event data were collected while the cells were under continuous cycling [21]. Neutron diffraction data were sliced (every 3600 s) and reduced by the VDRIVE software [22]. Single peak refinements were carried out using the GSAS [23] program.

2.4. Ex-situ neutron powder diffraction

Neutron powder diffraction patterns were collected for the lithium excess materials $Li[Li_{0.2}Ni_{0.2}Mn_{0.6}]O_2$ and chemically delithiated lithium excess sample using beamline HB2A [24] at the High Flux Isotope Reactor (HFIR) at Oak Ridge National Laboratory. Samples were loaded in a hermetically sealed holder to prevent air exposure. A monochromatic incident wavelength of 1.54 Å was chosen. Full pattern Rietveld refinement was performed using the GSAS [23] programs with the EXPGUI [25] interface.

3. Results and discussion

3.1. Cathode in $Li[Ni_{1/3}Mn_{1/3}Co_{1/3}]O_2$/C pouch cell

Fig. 2(a)–(c) shows the charge/discharge curve with surface contour plots of $LiNi_{1/3}Mn_{1/3}Co_{1/3}O_2$ (102), (108) and (110) ND peaks evolution as a function of time. The hydrogen atoms due to the presence of a large volume of electrolyte and separator materials contribute to the large fraction of the background, which reduces the signal-to-noise ratio. Other components in the pouch cell, such as the Al and Cu current collectors have crystalline features and cause ND peak overlap. These factors forced the use of single peak refinement to prevent erroneous full profile fitting results. Since both the cathode and anode material have a hexagonal lattice, d_{hkl} can be calculated by using the equation below:

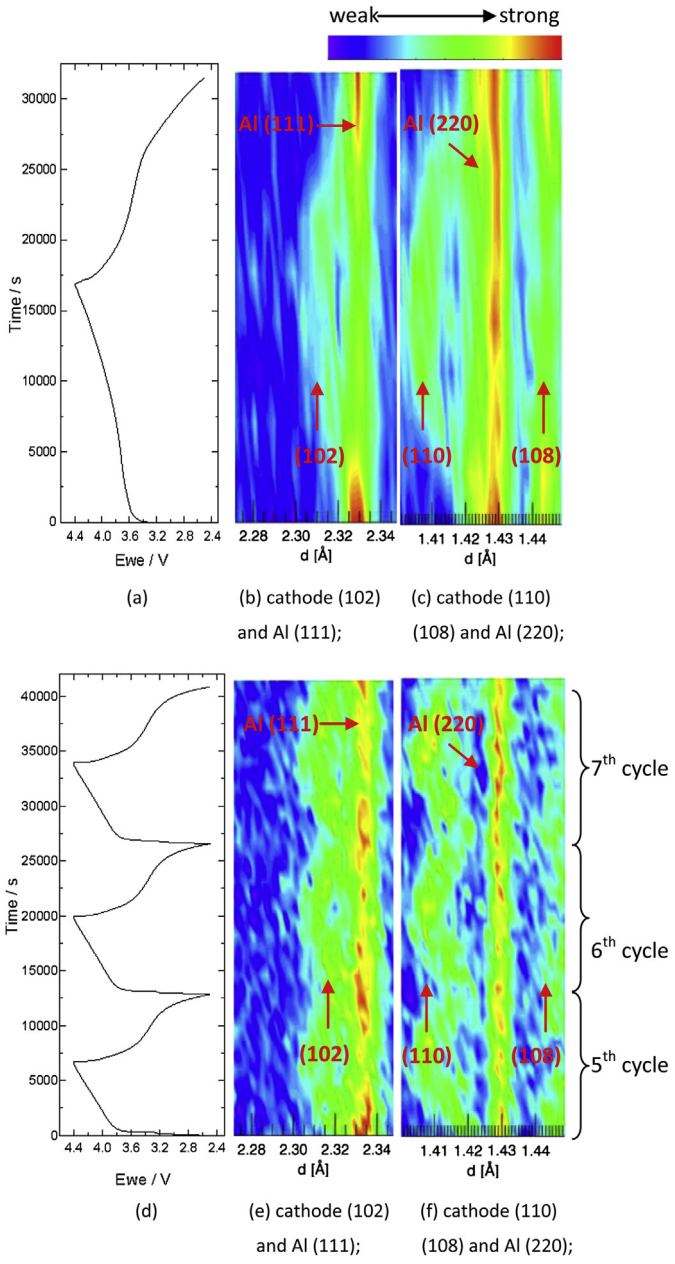

Fig. 2. (a): 1st cycle charge/discharge curve of $Li[Ni_{1/3}Mn_{1/3}Co_{1/3}]O_2$ and surface contour plots of (b)-(c): 1st cycle $Li[Ni_{1/3}Mn_{1/3}Co_{1/3}]O_2$ (102), (110) and (108); (d): 5–7th cycles charge/discharge curve of $Li[Ni_{1/3}Mn_{1/3}Co_{1/3}]O_2$ and surface contour plots of (e)–(f): 5–7th cycles $Li[Ni_{1/3}Mn_{1/3}Co_{1/3}]O_2$ (102), (110) and (108) neutron diffractions.

$$1/d_{hkl} = \left\{4/3^*\left[\left(h^2 + hk + k^2\right)/a^2\right] + l^2/c^2\right\}^{1/2}$$

Fsig. 4a is *a*- and *c*-lattice parameters evolution during cycling. During charging, Li^+ is extracted from the layered structure, at the same time Ni^{2+} is oxidized to Ni^{4+} which leads to ionic radii decreasing (e.g. r $Ni^{3+} = 0.60$Å, r $Ni^{4+} = 0.48$Å), as a consequence *a*-lattice parameter contracted monotonously. The removal of Li^+ introduces a concentration gradient and electrostatic repulsion from adjacent oxygen layers accounting for the increased *c*-lattice parameter [26]. The (108) peak remains unchanged while (110) decreased rapidly when Li ions are extracted, and at the end of charge (110) planes have the shortest distance. The (108) plane corresponds to the out-of-plane periodicity, which intersects 1 in

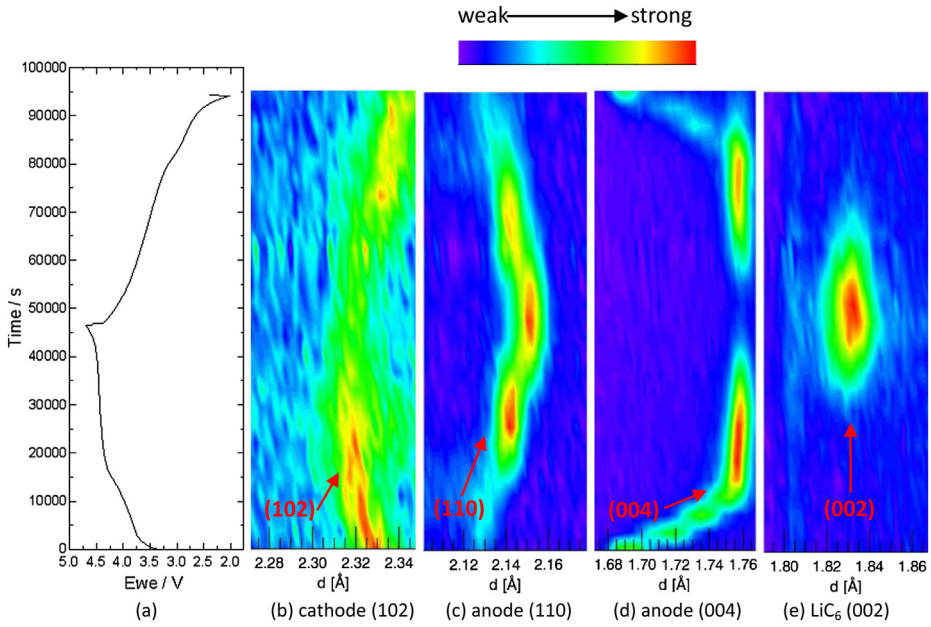

Fig. 3. (a): 1st cycle charge/discharge curve of $Li[Li_{0.2}Ni_{0.18}Mn_{0.53}Co_{0.1}]O_2$ and surface contour plots of (b): $Li[Li_{0.2}Ni_{0.18}Mn_{0.53}Co_{0.1}]O_2$ (102); (c): Li_xC_6 (110); (d): Li_xC_6 (004); (e): LiC_6 (002) neutron diffractions.

every 8 transition metal (TM) or Li^+ layers (along the *c*-axis). The out-of-plane lattice spacing changes correspond strongly to the *c*-lattice parameter. As ***l*** increases in the (10***l***) family of peaks, the d_{10l} shift decreases in magnitude. Since ***l*** here equals to 8 the change of *c* only brings negligible change of d_{108}. The (110) plane depends strongly on *a*-lattice parameter, illustrating strong anisotropy in the material during electrochemical cycling. At the beginning of the charge $a = 2.852 \pm 0.001$ Å, $c = 14.173 \pm 0.0008$ Å which are close to the reported results, [3] and the trends upon charge are consistent with previous work [27]. The discharge is a process of Li^+ reinserting into the layered structure. After discharge, *a*- and *c*-parameter return to $a = 2.851 \pm 0.001$ Å, $c = 14.179 \pm 0.0006$ Å illustrating a completely reversible intercalation mechanism. Fig. 2(e) and (f) show the (102), (110) and (108) peaks in the following cycles, only 5–7th cycles data were collected due to beam off during 2nd–4th cycles. But we can clearly see the (108) remains unchanged, while (102) and (110) repeatedly decrease during charge and increase during discharge.

3.2. $Li[Li_{0.2}Ni_{0.18}Mn_{0.53}Co_{0.1}]O_2$/C pouch cell

As a comparison study, the structural changes of the Li $[Li_{0.2}Ni_{0.18}Mn_{0.53}Co_{0.1}]O_2$ cathode and graphite anode during first electrochemical cycle were observed. The pouch cell has a characteristic sloping region up to 4.3 V and a plateau region at 4.4 V. The charge capacity is more than 250 mAh g^{-1}, discharge capacity is more than 200 mAh g^{-1} due to irreversible capacity loss in the first cycle. The capacity before 4.3 V is more than 90 mAh g^{-1}, suggesting that most of the Co^{3+} has been oxidized to Co^{4+}.

Fig. 3(a)–(e) shows the charge/discharge curve with several selected ND peaks visually depicted as surface contour plots to show the peak evolution as a function time. Due to the limited amount of active materials in the beam, only the evolution of (102) peak of $Li[Li_{0.2}Ni_{0.18}Mn_{0.53}Co_{0.1}]O_2$ has been observed. Fig. 4b is the single peak refinement results for d_{102} change during the first electrochemical cycle. In the slope region before 4.3 V, d_{102} decreased rapidly from 2.326 ± 0.0005Å to 2.318 ± 0.0006 Å, corresponding to the Ni^{2+}/Ni^{4+} and Co^{3+}/Co^{4+} redox reaction. As aforementioned, when Li^+ is extracted from the layered structure, Ni^{2+} is oxidized to Ni^{4+} and Co^{3+} is oxidized to Co^{4+} which results in a decrease in the ionic radii of these ions and a larger repulsion from the adjacent oxygen layers. After the slope region a plateau region is observed, in this region the d_{102} spacing decreased slightly by 0.002 ± 0.0005Å. During discharge, Li^+ is reinserted into the structure, subsequently the d_{102} spacing increases monotonically. At the end of first cycle, d_{102} is 2.338 ± 0.0006Å which is larger than the pristine value. Although it is hard to distinguish how the *a*- and *c*-lattice parameters have changed after the first electrochemical cycle, it is obvious that the volume of the lattice has increased, which is consistent with previous reports [7,12].

Compared to the cathode, the graphite anode shows stronger peaks such as the (112), (110), (100), (004) and (006). Fig. 3(c)–(e) only shows the Li_xC_6 (004) and (110) peak. Since several *in-situ* ND studies have previously reported the structural changes seen with the graphite anode [15,28], it will not be discussed in detail here. By looking at Fig. 3(c)–(e), at the end of charge, the Li_xC_6 (004) peak becomes weak while LiC_6 (002) peak starts to appear, indicating a phase transformation process. The phase change process is also indicated by Li_xC_6 (110) peak, at the middle stage of charge LiC_{12} phase formed, then gradually transforms to LiC_6 phase as more Li^+ inserted into the anode. In the current cell design there is 25% excess graphite anode, so at the end of charge we should have a mixed phase between Li_xC_6 and LiC_6. Neeraj Sharma [15] also observed a two phase system at end of charge for their *in-situ* ND study on the $LiCoO_2$/C system. Fig. 4c shows the calculated graphite lattice parameters during the first charge/discharge process. At the beginning of the 1st charge, the *a*-parameter of the graphite anode is 2.458 ± 0.0017 Å and the *c*-parameter is 6.776 ± 0.0004 Å (distance between carbon layers equals *c*/2), while at the end of charge it undergoes a phase change to LiC_6 phase coupled with a large increase in the *a*-parameter of 4.304 ± 0.0003 Å and the *c*-parameter of 3.666 ± 0.0003 Å (distance between carbon layers equals *c*), which is consistent with previous work [29,30]. During discharge, as Li^+ is extracted from the graphite layer the LiC_6 phase disappeared. At the end of the discharge the *a*-parameter of the Li_xC_6 phase goes back to 2.462 ± 0.0024 Å slightly larger than the pristine which is 2.458 ± 0.0017 Å, possibly because of the irreversible Li^+ in the graphite. In another word, the structure of anode

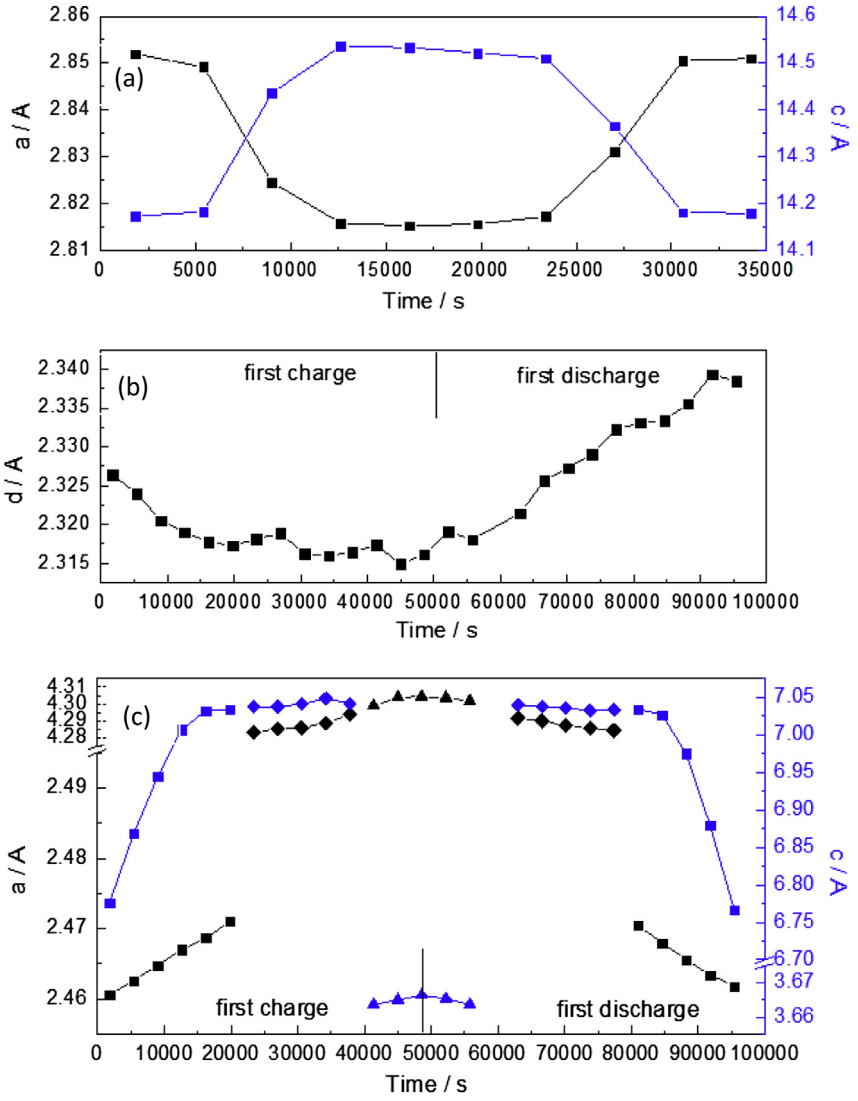

Fig. 4. (a): Cathode $Li[Ni_{1/3}Mn_{1/3}Co_{1/3}]O_2$ lattice parameters change during 1st cycle, black is the a-parameter, blue is the c-parameter; (b): $Li[Li_{0.2}Ni_{0.18}Mn_{0.53}Co_{0.1}]O_2$ (102) d-spacing change during 1st cycle; (c): Anode graphite lattice parameter change during 1st cycle, black is the a-parameter, blue is the c-parameter, the square is the Li_xC_6 phase, the diamond is the LiC_{12} phase, the triangle is the LiC_6 phase. (For interpretation of the references to color in this figure legend, the reader is referred to the web version of this article.)

is reversible during electrochemical cycle. The ability of monitoring the dynamic structural changes in cathode and anode simultaneously is another strong merit of neutron scattering technique.

3.3. *Ex-situ neutron diffraction on* $Li[Li_{0.2}Ni_{0.2}Mn_{0.6}]O_2$

As a complementary experiment of *in-situ* neutron study of lithium-excess layered oxide material, *ex-situ* neutron diffractions were carried out on lithium-excess material $Li[Li_{0.2}Ni_{0.2}Mn_{0.6}]O_2$. Chemical delithiation was designed to simulate the charge process where a large amount of Li is extracted from the structure.

Chemical delithiation was designed to remove 0.8 mol of Li^+ from $Li[Li_{0.2}Ni_{0.2}Mn_{0.6}]O_2$ by using NO_2BF_4. After 0.4 mol of Li^+ removed from the structure, all the Ni^{2+} were oxidized to Ni^{4+}. The rest 0.4 mol Li^+ were assumed to be removed in the form of Li_2O. Neutron diffraction patterns of the pristine sample and chemically delithiated sample are shown in Fig. 5 and refined using a single R-3m phase. The superlattice peaks between 20 and 30°(2θ) can be seen in both samples. Such superstructure peaks are associated with a honeycomb ordering of Li, and transition metals in the TM layers [4,5]. The superlattice peaks can be seen more clearly in the chemically delithiated sample. It is possible that the irreversible loss of oxygen increased the contrast between the superlattice peaks and main peaks. These peaks cannot be fitted by using R-3m space group. According to previous study of layered oxides [31], we used C/2m and $P3_112$ space groups to do the pattern matching (see support information Figure S1–S4). By applying C/2m and $P3_112$ space group, not only these superlattice peaks, but also other peaks can be fitted, e.g. the peak at 42°. Although these peaks can be fitted using the C/2m or $P3_112$ space groups, refinement of the structural model is lacking due to large amounts of defects originating from chemical delithiation oxygen vacancies. We propose that chemical delithiation creates large amounts of site disorder as well as structural defects within the lithium-excess material that prohibit simple structural refinement using a single R-3m, C2/m or $P3_112$ space group. In order to refine the pattern quantitatively, more work has to be done to identify the suitable structure model.

Rietveld refinement of the chemically delithiated structure used a single R-3m space group excluding the superlattice range and was based on 0.4 mol Li^+ in the structure ($Li_{0.4}Ni_{0.2}Mn_{0.6}O_{1.8}$). After delithiation, the lattice parameter *a* decreased 0.008 Å, while the lattice parameter *c* increased 0.0141 Å due to Ni oxidation from Ni^{2+}

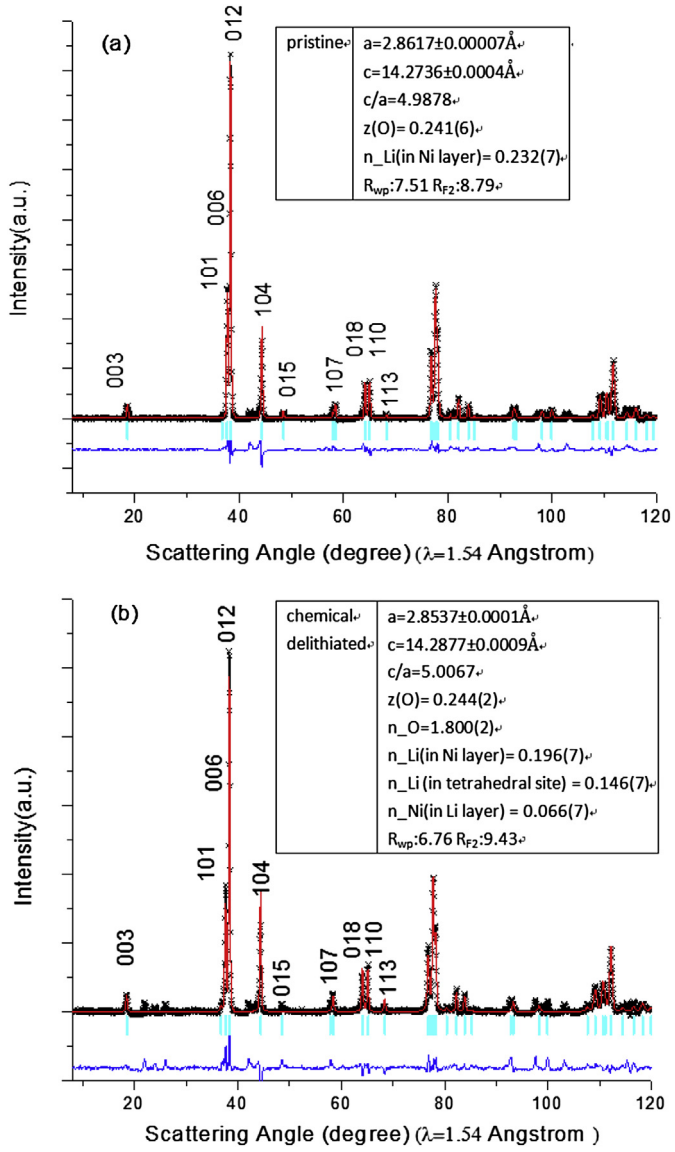

Fig. 5. *Ex-situ* neutron diffraction patterns and Rietveld Refinement results: (a) pristine $Li[Li_{0.2}Ni_{0.2}Mn_{0.6}]O_2$; (b) chemically delithiated sample $Li_{0.4}Ni_{0.2}Mn_{0.6}O_{1.8}$.

to Ni^{4+} causing increased repulsion between the adjacent oxygen layers. These changes are not as large as previous reports possibly due to the presence of other phases existing as defects as evidenced by the group of superlattice peaks. The large amounts of Li^+ vacancies as well as the increased *c*-lattice spacing facilitate Ni interlayer migration accounting for the increase from 3.27% to 6.67% following delithiation. Furthermore, Rietveld refinement also identified 20% oxygen deficiency in the single R-3m phase model. These vacancies created in the oxygen layers enable Li/Ni cation migration by hopping through nearby vacancies. Refinement of the neutron pattern of the delithiated structure identified the formation of tetrahedral Li^+ sites. The use of chemical delithiation combined with neutron diffraction proves to be a powerful method to identify structural changes which correlate to those proposed from electrochemical delithiation [9,32].

4. Conclusion

In this work, a lab pouch cell was designed for *in-situ* Neutron diffraction in order to study two high capacity cathode materials in the layered oxides family: classical layered oxide $LiNi_{1/3}Mn_{1/3}Co_{1/3}O_2$ and lithium excess layered oxide $Li[Li_{0.2}Ni_{0.18}Mn_{0.53}Co_{0.1}]O_2$. By using a single peak refinement technique, structural changes of these two materials are observed quantitatively. Li excess layered oxide $Li[Li_{0.2}Ni_{0.18}Mn_{0.53}Co_{0.1}]O_2$ shows an irreversible volume expansion after the first cycle which is most likely caused by oxygen loss from the structure, while classical layered oxide $LiNi_{1/3}Mn_{1/3}Co_{1/3}O_2$ retains the reversible structure in the electrochemical voltage window. Anisotropy in the *a*- and *c*-lattice directions are observed. *Ex-situ* neutron diffraction experiments on lithium-excess material also reveal irreversible changes of structure after chemical delithiation. Major efforts are currently underway to improve the *in-situ* neutron scattering data quality to enable full Rietveld refinement of atomic positions. In addition to having the ability to monitor the dynamic changes in the cathode, our setup allows for the simultaneous observation of the anode material. Our observation shows a phase transformation in the anode at end of charge and start of discharge. The reversible change of structure and phase transformation shows good reversibility performance of the graphite anode.

Acknowledgment

The neutron experiments benefit from the SNS and HFIR user facilities sponsored by the office of Basic Energy Sciences (BES), the Office of Science of the U.S. Department of Energy (DOE). H. Liu acknowledges the financial support from China Scholarship Council under Award Number 2011631005. UCSD's efforts are supported by the Assistant Secretary for Energy Efficiency and Renewable Energy, Office of Vehicle Technologies of the U.S. DOE under Contract No. DE-AC02-05CH11231, Subcontract No. 7056412 under the Batteries for Advanced Transportation Technologies (BATT) Program. L. Cai acknowledges the financial support from the Division of Materials Science, the office of BES, Office of Science of DOE.

Appendix A. Supplementary data

Supplementary data related to this article can be found at http://dx.doi.org/10.1016/j.jpowsour.2013.04.149.

References

[1] T. Ohzuku, Y. Makimura, Chemistry Letters (2001) 642–643.
[2] N. Yabuuchi, T. Ohzuku, Journal of Power Sources 119 (2003) 171–174.
[3] S.C. Yin, Y.H. Rho, I. Swainson, L.F. Nazar, Chemistry of Materials 18 (2006) 1901–1910.
[4] W.S. Yoon, S. Iannopollo, C.P. Grey, D. Carlier, J. Gorman, J. Reed, G. Ceder, Electrochemical and Solid-State Letters 7 (2004) A167–A171.
[5] P. Strobel, B. Lambertandron, Journal of Solid State Chemistry 75 (1988) 90–98.
[6] C.S. Johnson, J.S. Kim, C. Lefief, N. Li, J.T. Vaughey, M.M. Thackeray, Electrochemistry Communications 6 (2004) 1085–1091.
[7] Z. Lu, J.R. Dahn, Journal of The Electrochemical Society 149 (2002) A815.
[8] M.M. Thackeray, S.-H. Kang, C.S. Johnson, J.T. Vaughey, R. Benedek, S.A. Hackney, Journal of Materials Chemistry 17 (2007) 3112.
[9] A.R. Armstrong, M. Holzapfel, P. Novak, C.S. Johnson, S.H. Kang, M.M. Thackeray, P.G. Bruce, Journal of the American Chemical Society 128 (2006) 8694–8698.
[10] B. Xu, C.R. Fell, M. Chi, Y.S. Meng, Energy & Environmental Science 4 (2011) 2223.
[11] A.D. Robertson, P.G. Bruce, Electrochemical and Solid-State Letters 7 (2004) A294.
[12] C.R. Fell, M. Chi, Y.S. Meng, J.L. Jones, Solid State Ionics 207 (2012) 44–49.
[13] A. Ito, Y. Sato, T. Sanada, M. Hatano, H. Horie, Y. Ohsawa, Journal of Power Sources 196 (2011) 6828–6834.
[14] N. Sharma, V.K. Peterson, Journal of Solid State Electrochemistry 16 (2011) 1849–1856.
[15] N. Sharma, V.K. Peterson, M.M. Elcombe, M. Avdeev, A.J. Studer, N. Blagojevic, R. Yusoff, N. Kamarulzaman, Journal of Power Sources 195 (2010) 8258–8266.
[16] H. Berg, H. Rundlov, J.O. Thomas, Solid State Ionics 144 (2001) 65–69.
[17] L. Cai, K. An, Z. Feng, C. Liang, S.J. Harris, Journal of Power Sources 236 (2013) 163–168.
[18] J.F. Colin, V. Godbole, P. Novak, Electrochemistry Communications 12 (2010) 804–807.

[19] X.L. Wang, K. An, L. Cai, Z.L. Feng, S.E. Nagler, C. Daniel, K.J. Rhodes, A.D. Stoica, H.D. Skorpenske, C.D. Liang, W. Zhang, J. Kim, Y. Qi, S.J. Harris, *Scientific Reports* UK 2 (2012). Article number: 747.
[20] C.R. Fell, K.J. Carroll, M. Chi, Y.S. Meng, Journal of The Electrochemical Society 157 (2010) A1202.
[21] K. An, H.D. Skorpenske, A.D. Stoica, D. Ma, X.L. Wang, E. Cakmak, Metallurgical and Materials Transactions A 42A (2011) 95–99.
[22] K. An, ORNL Report, Oak Ridge National Laboratory, 2012. ORNL-TM-2012-621.
[23] A.C. Larson, R.B.V. Dreele, Los Alamos National Laboratory Report (LAUR), 86-748 (2004).
[24] V.O. Garlea, B.C. Chakoumakos, S.A. Moore, G.B. Taylor, T. Chae, R.G. Maples, R.A. Riedel, G.W. Lynn, D.L. Selby, Applied Physics A Materials and Processing 99 (2010) 531–535.
[25] B.H. Toby, Journal of Applied Crystallography 34 (2001) 210–213.
[26] W. Senaratne, K. Takada, R. Das, J. Cohen, B. Baird, H.D. Abruna, C.K. Ober, Biosensors & Bioelectronics 22 (2006) 63–70.
[27] J.-M. Kim, H.-T. Chung, Electrochimica Acta 49 (2004) 937–944.
[28] M.A. Rodriguez, D. Ingersoll, S.C. Vogel, D.J. Williams, Electrochemical Solid State Letters 7 (2004) A8–A10.
[29] M. Winter, J.O. Besenhard, M.E. Spahr, P. Novak, Advanced Materials 10 (1998) 725–763.
[30] D. Guerard, A. Herold, Carbon 13 (1975) 337–345.
[31] Y.S. Meng, G. Ceder, C.P. Grey, W.S. Yoon, Y. Shao-Horn, Electrochemical and Solid-State Letters 7 (2004) A155.
[32] C.R. Fell, D. Qian, K.J. Carroll, M. Chi, J.L. Jones, S. Meng, Chemistry of Materials 25 (2013) 1621–1629.